

A REVIEW OF VORTEX SHEDDING RESEARCH AND ITS APPLICATION

ROGER KING

BHRA Fluid Engineering, Cranfield, Bedford MK43 0AJ, England

Abstract—This paper is a review of research work with cylinders in steady currents. The emphasis is mainly on cylinders in water, particularly the research undertaken at BHRA and its general application. Comparisons are made with the work of other authors for both water and air flow and over 60 references are reviewed. The mechanisms of flow-excited oscillations are discussed for isolated vertical and inclined cylinders. The effects of length/diameter ratio, cylinder surface roughness and channel blockage are presented. Wake interactions caused by cylinder-cylinder and cylinder-splitter arrangements are detailed. The results of tests with pane and three-dimensional frames are described and quantified in terms of isolated cylinder data.

The paper closes with a section describing methods of avoiding oscillations by calculation at the design stage or by the use of clamp-on devices for completed structures in water flow.

1. INTRODUCTION

WHEN a fluid flows about a stationary cylinder the flow separates, vortices are shed and a periodic wake is formed. The frequency (f) of pairs of vortices is a function of velocity (V) cylinder diameter (d) and Reynolds number (Re). S , the non-dimensional wake Strouhal number is defined as $S = f_v d / V$, and over a wide range of Reynolds numbers $10^3 < Re < 10^5$, $S \approx 0.2$. The general relationship between S and Re is well documented (1), Fig. 1, but absolute values of S also depend upon cylinder surface roughness, length/diameter ratio and turbulence levels. (See 2.6).

Each time a vortex is shed from the cylinder, it alters the local pressure distribution, and the cylinder experiences a time-varying force at the frequency of vortex shedding.

If the cylinder is flexible or flexibly mounted, interactions can arise between the vortex shedding mechanism and the cylinder deflections. Under certain conditions, sustained oscillations can be excited and the cylinder oscillates at a frequency close to, or coincident with, its natural frequency. Such oscillations are classed as self-excited, or self-controlled.

In air flow, chimneys, telegraph wires and pipeline suspension bridges oscillate almost invariably in a direction normal to the flow of air. These are the so-called crossflow oscillations. There have been rare exceptions when cylinders in air flow have oscillated in the direction of flow (i.e. in-line motion) but these have been due to peculiarities of their installation (2, 3). In water, marine piles, submarine periscopes and braced members of offshore structures can be excited to oscillate in both the in-line and cross-flow directions (4). The in-line oscillations can be excited at flow velocities much lower than the critical velocities for cross-flow motion. The differences between the onset of cylinder motion in the two fluid media is probably due to differences in energy balances within the two systems. However, Richardson (5) quotes Bénard as maintaining that the 'spacing and disposition of vortices in air flow do not conform to those in water flow'; this has not been substantiated generally and must be considered rather unlikely.

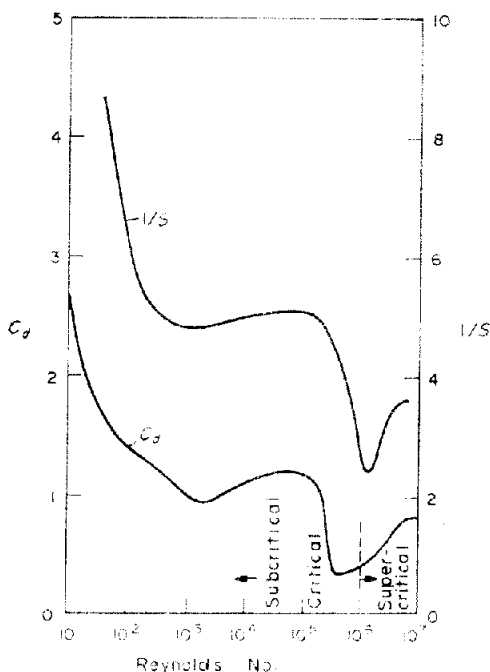


FIG. 1. General relationships between Strouhal number, steady drag coefficient and Reynolds number.

2. GENERAL REVIEW OF RESEARCH

Background

Aerodynamicists usually rank experimental data by relating non-dimensional oscillatory amplitudes (y/d) to the two non-dimensional groups Reduced Velocity V/nd (n = cylinder natural frequency) and the Stability Parameter $K_s = 2m_e\delta/\rho d^2$ (m_e is the equivalent mass/unit length, δ is the logarithmic decrement and ρ is the mass density of the fluid). This practice will be followed here.

It will be noted that Reduced Velocity and Strouhal number are related; a Reduced Velocity of 5 is the inverse of the Strouhal number S for the condition $f_v = n$. For values of V/nd less than 5, f_v is less than n ; conversely for a V/nd value greater than 5, f_v is greater than n . Similarly, K_s can be interpreted as an amalgamation of the mass ratio $m_e/\rho d^2$ and the logarithmic decrement δ . This grouping results from the energy balance at resonance (6).

The variation of oscillatory amplitudes of cylinders with variation of mass ratio and damping has been investigated by several authors (4, 7-9). Generally, it is agreed that within limits the amplitudes could be correlated through equality of the product $m_e\delta$. King (10) demonstrated the close agreement between hydroelastic model results and fullscale site tests of marine piles, using the oscillatory amplitudes, V/nd , and K_s as bases of comparison. The Reynolds numbers of the two sets of results differed considerably and the agreement between the model and fullscale behaviour is explained by reference to the comparative uniformity of the apparent Strouhal number of oscillating cylinders (10).

The absolute values of V/nd for excitation of sustained oscillations are also influenced by length/diameter effects (see Section 2.1) and the proximity of sidewalls.

2.1 Correlation length, cylinder length and threshold amplitudes

There is considerable evidence to show that vortices are shed in cells from stationary cylinders; the length of each cell is termed the correlation length. Absolute values vary with Reynolds number, turbulence, length/diameter ratio, and surface roughness. Typical values are summarised in Table 1 below:

TABLE 1. CORRELATION LENGTHS AND REYNOLDS NUMBERS OF SMOOTH CYLINDERS

Reynolds number	Correlation length	Source
$40 < Re < 150$	$15d-20d$	(11)
$150 < Re < 10^3$	$2d-3d$	(11)
$1.1 \times 10^3 < Re < 4.5 \times 10^4$	$3d-6d$	(12)
$\geq 10^5$	$0.5d$	(11)
2×10^5	$1.56d$	(13)

If the cylinder is long compared with the correlation length, not all vortices cause forces in phase with each other, resulting in a reduction in the net oscillating force. Keefe (14) was able to vary the oscillatory forces on a cylinder by attaching concentric discs perpendicular to it. A decrease in disc spacing from $18d$ to $3d$ increased the oscillatory forces by 35% and it must be concluded that the discs split the cylinder into a series of well correlated, contiguous sections.

The correlation length is increased (15) when the cylinder oscillates with an amplitude greater than a certain proportion of the cylinder diameter. This is termed the threshold amplitude. The threshold amplitude for cross-flow oscillations is 10% of a diameter (16). King and Every (17) showed that the threshold amplitude of in-line oscillations is between 1% and 2% of a diameter. The maximum amplitudes possible for the cross-flow and in-line directions are about 2 diameters and 0.2 diameters and the threshold amplitudes are similar proportions of the respective maxima. Additionally, the oscillatory force/unit length for long cylinders is less than for short cylinders, when the oscillatory amplitude is small. As the amplitude is increased, the oscillatory force/unit length increases more rapidly for long cylinders than for short cylinders, until at some amplitude the forces become approximately equal (11). The implication is that the cylinder oscillations must re-organise the vortex shedding process. In particular, the re-organisation would be most evident for long cylinders, where initially there would be many regions of out of phase vortex shedding.

Gowda (8) presented the results of wind tunnel tests with cylinders of varying length, with and without end plates. He proposed a value of $L/d \approx 45$ for freedom from end effects (Bénard (18) suggested $L/d \approx 27$). Figure 2, taken from Gowda, shows the variation of vortex shedding frequency with variation of cylinder length. For cylinders with three-dimensional flow effects (end effects) the shedding frequency is consistently lower than for the two-dimensional cylinder (with end plates) except for $L/d \geq 50$; for cylinders of $L/d \approx 15$, the shedding frequency is 35% lower than for the infinite cylinder case.

Gowda also investigated the effects of sizes of end plates on vortex shedding frequency showing that for a cylinder of $L/d = 18$, the diameter of the end plates should be at least $10d$ to avoid all end effects.

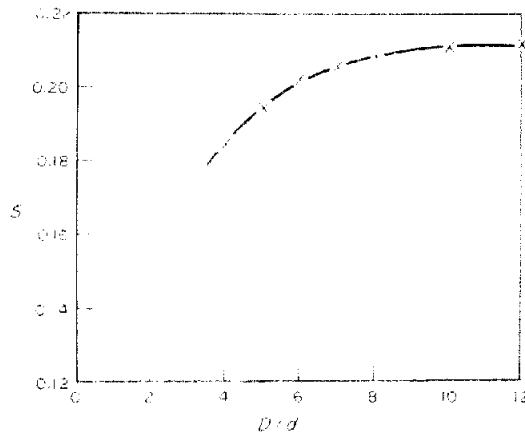


FIG. 2(a). The influence of end-plates upon vortex shedding.

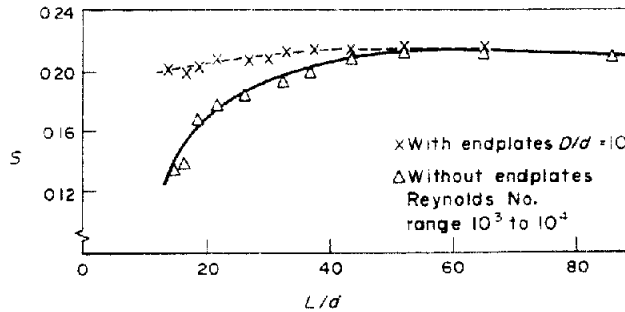


FIG. 2(b). The influence of stationary cylinder L/d upon vortex shedding.

2.2 Lock-in or synchronisation of vortex shedding

Having introduced the Strouhal number of a stationary cylinder and shown the velocity-dependence of the vortex shedding frequency, we can consider the dominant wake frequencies of both stationary and self-excited cylinders.

Lock-in is the phenomenon whereby the cylinder motion apparently controls the vortex shedding frequency. Over a range of velocities the cylinder oscillates at or near its natural frequency and the vortex shedding is synchronised with this frequency (19, 20).

In a series of laboratory tests (4) several interesting aspects of cylinder/wake interaction were recorded. Long cylinders were mounted as vertical cantilevers from the bed of a water channel; strain gauges glued to their surfaces sensed the cylinders' response to vortex shedding. Thermistor probes were placed in the wake to detect dominant frequencies.

Figure 3(a) shows the dominant wake frequencies for a range of velocities. Initially, as the velocity is increased from zero, the cylinder is stationary and the vortex shedding frequency detected by the thermistor probes follows the $S = 0.2$ straight line relationship. However, as the lower critical velocity is approached, the cylinder begins to oscillate and the dominant wake frequency shifts from the $S = 0.2$ line and remains nominally equal to

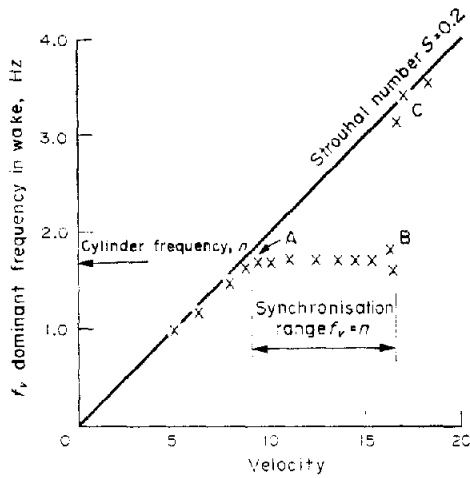


FIG. 3(a). Lock-in or synchronisation of vortex shedding crossflow oscillations.

the cylinder's natural frequency (indicated by the arrow). Lock-in occurs over a wide range of velocities (point A to point B), and the recorded vortex shedding frequency coincides approximately with the natural frequency of the cylinder. The cylinder oscillations vary from the still-water natural frequency, being slightly lower at the onset of oscillations and slightly higher at the upper critical velocity (point B). At a velocity only marginally above the upper critical, (C) the cylinder's large amplitude motion ceases and the vortex shedding frequency returns to the value predicted by the $S = 0.2$ straight line for a stationary cylinder. The trace of Fig. 3(b) was recorded from the virtually stationary cylinder at the velocity corresponding to C. A comparison of the strain gauge outputs from the middle and base of the cylinder reveals a lack of similarity between the motion of these sections, indicating a variation in phase and frequency of the exciting forces along the cylinder length which is apparently consistent with the concept of the vortices shed in cells from pseudo-stationary cylinders.

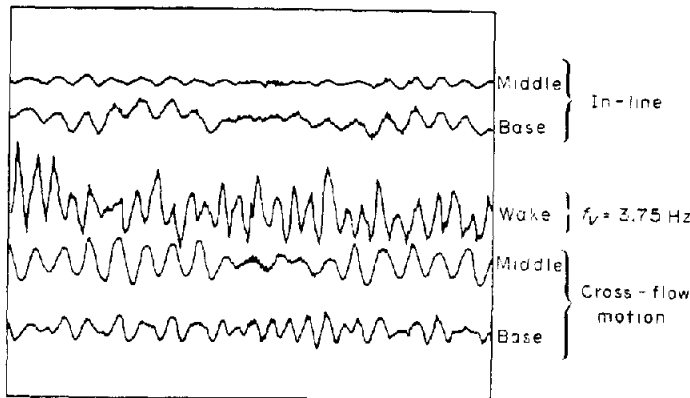


FIG. 3(b). Loss of correlation at the end of lock-in (Point C on Fig. 3(a)).

Gowda (8) showed that L/d effects influenced the V/nd values at which oscillations were initiated. Generally, cylinders of finite length were excited at lower velocities than those of infinite length. This is rather surprising since Gowda previously showed that L/d also affected the vortex shedding frequency (Section 2.1) and it would seem logical to expect that the augmentation of the lower frequency Strouhal vortex shedding of the three-dimensional cylinder would be achieved by increasing the velocities (and thus V/nd) to produce lock-in.

Figure 4 lists the different types of cross-flow oscillation for a range of damping levels (20). In Fig. 4(a) the amplitude remains below the threshold and fails to control the wake frequency. The response is small, and forced at the Strouhal vortex shedding frequency. In the middle figure the previously described (4) synchronisation occurs over a small velocity range although the amplitude is well below the threshold quoted by (16). On each side of the resonant amplitude response, the cylinder is forced to oscillate at the Strouhal vortex

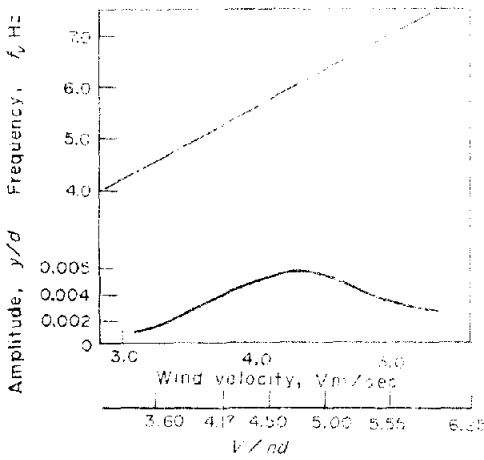


FIG. 4(a). High damping.

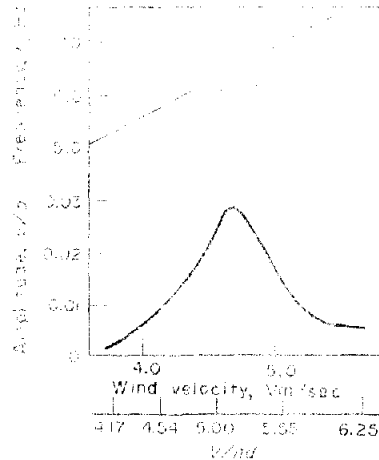


FIG. 4(b). Medium damping.

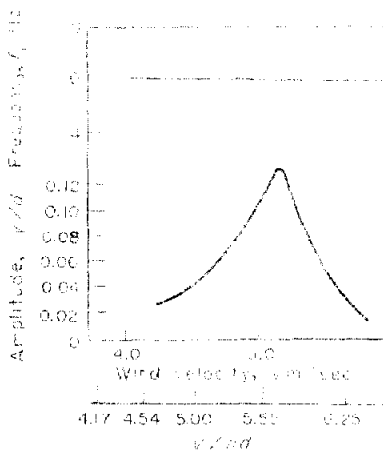


FIG. 4(c). Light damping.

FIG. 4. Variation of amplitude response with damping.

shedding frequency. Finally, Fig. 4(c) shows the response of a very lightly damped cylinder; the cylinder oscillates at its natural frequency over a comparatively wide velocity range, and this may be regarded as a magnification of the middle portion of the amplitude response in Fig. 4(b).

The wake frequency and cylinder motion traces of the first and second instability regions in-line are shown in Fig. 5. As for the cross-flow direction, the vortex shedding frequency

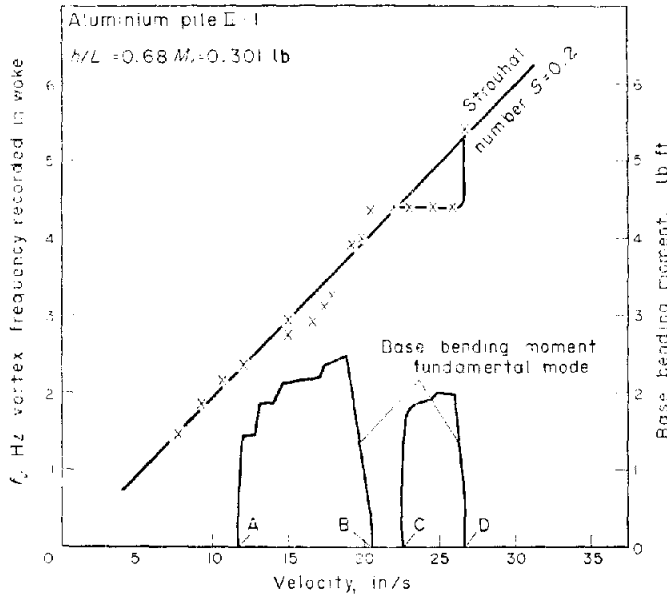


FIG. 5. Vortex shedding frequencies; self-excited oscillations of the cylinder in the in-line direction.

initially follows the $S = 0.2$ line and the cylinder remains virtually stationary. At point A ($V/nd = 1.7$) the cylinder begins to oscillate at its natural frequency in the in-line direction and this first instability region extends until point B ($V/nd = 2.3$). Between these two velocities the dominant wake frequency deviates only marginally from the $S = 0.2$ line. Thus, although the cylinder is oscillating, the wake is similar to that shed from a stationary cylinder. The two nearly symmetric vortices are shed simultaneously once each cycle as the cylinder reverses into the flow direction. The symmetric arrangement of vortices is theoretically unstable (21) and this is borne out in practice; they coalesce to form a staggered alternate street with a frequency predicted from the Strouhal number at the velocity considered. The coalescence takes place immediately downstream from the cylinder and the early stages can be seen clearly in Fig. 11. This shows the two approximately symmetric vortices being shed from the cylinder, and three alternate vortices formed by the coalescence of symmetric vortices from previous cycles of motion.

It has been shown (4) that throughout the first instability region, the ratio of cylinder frequency to dominant wake frequency (n/f_v) apparently slips into 'convenient' numbers. It will be remembered that V/nd can be regarded as a ratio of cylinder frequency to vortex shedding frequency; at $V/nd = 1.25$ (the onset of oscillations) $n/f_v = 4$; at higher velocities

the ratios change through 7 : 2, 3 : 1, 7 : 3, 13 : 6, until finally at $V/nd = 2.5$ (the end of the instability region), the ratio n/f_v is 2. This could account for the 'steps' in the outline shapes of the response curves for the first instability region as shown in Fig. 5. Figure 6

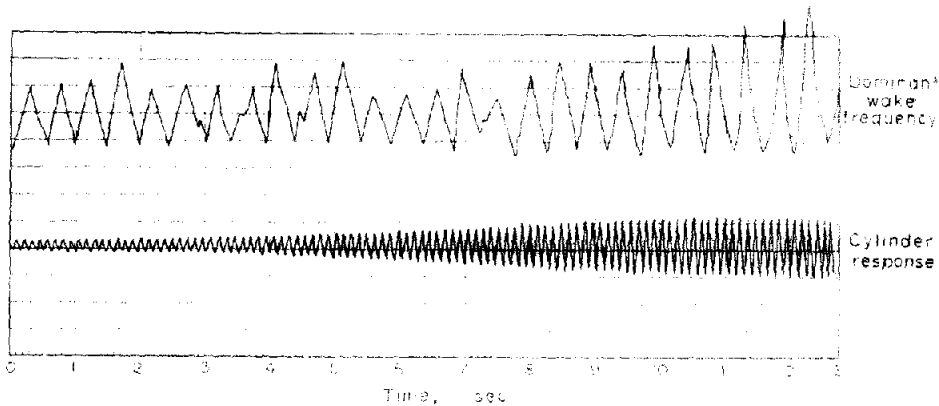


FIG. 6. The onset of instability in-line.

shows the onset of oscillations and the dominant wake frequencies. Note that the onset occurs at $V/nd = 1.25$ and this represents $n/f_v = 4$. The frequency of the wake is almost unaltered when compared with the stationary cylinder value but there is an increase in the magnitude of the wake signal owing to augmentation of the vortex circulation.

The second instability region in Fig. 5 extends from point C ($V/nd = 2.8$) to point D ($V/nd = 3.2$) and the dominant wake frequencies are comparatively constant throughout this region. Moreover, the dominant wake frequency is equal to one half the cylinder natural frequency, and the vortices are shed from alternate sides of the cylinder (Fig. 12). Force and surface pressure measurements on stationary rigid cylinders (22, 23) have indicated a 2 : 1 ratio between the frequencies of forces in the in-line and cross-flow directions at a given vortex shedding frequency. Thus, for lock-in to occur on the flexible cylinder in the second instability region, the in-line frequencies would be synchronised when $f_v = n/2$ (Fig. 5).

2.3 Logarithmic decrement and the initiation of in-line oscillations in water

If the free end of a circular cylinder in a depth, h , of still water is displaced and released, the cylinder oscillates freely with a gradually decreasing amplitude. The rate of decay of this transient, measured in terms of the logarithmic decrement is approximately constant and independent of amplitude effects for initial amplitudes of up to 0.5 diameters (24). This implies pseudo viscous damping. The logarithmic decrement in air (25) is produced by the structural material hysteretic damping and the comparatively insignificant air damping, approximating to viscous damping i.e., δ is constant. In a depth, h , of water, the total logarithmic decrement δ_t comprises the structural contribution (δ) and the viscous damping of the water (δ_h). This results in $\delta_t = \text{constant}$ for each water depth, natural frequency and cylinder geometry (24), i.e., $\delta_t = \delta + \delta_h$. The graph of Fig 7 demonstrates this effect, showing the way in which δ_h increases very rapidly for $h/L \geq 0.5$.

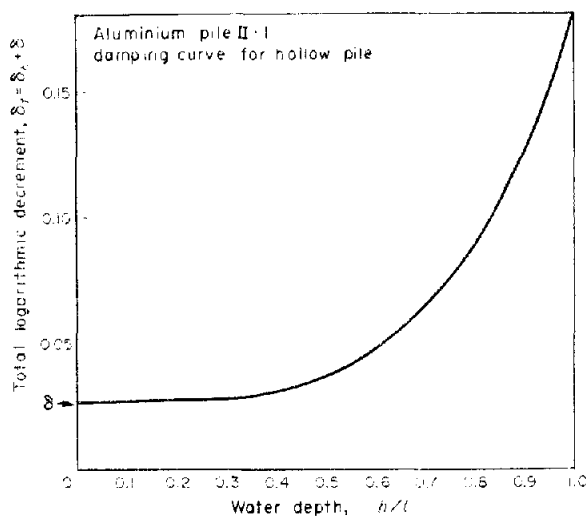


FIG. 7. Logarithmic decrement for a cylinder in varying still water depths.

When oscillations are initiated in flowing water, they do not occur instantaneously because finite time is necessary for the establishment of the interactions between vortex-shedding and the cylinder's flexibility. A typical u.v. trace of the onset of instability (Fig. 6) shows that the limiting amplitude is established after approximately 30–40 cycles (26). The initial rate at which the instability occurs is equivalent to a negative logarithmic decrement ($-\delta_e$) and for the trace shown, $-\delta_e = \delta_h$, where δ_h is a function of water depth. At the lower water levels the Stability Parameter K_s is larger and these higher values are associated with higher rates of instability. In a wind-tunnel (27) it has been demonstrated that a fairly heavily damped cylinder could suppress the excitation of small amplitudes whilst large amplitude motion was sustained after release from an initial displacement. This would represent the limiting condition for the $-\delta_e = 0$ rate of onset of instability.

The behaviour of a 'stable' cylinder (i.e. $K_s \approx 1.2$) in flowing water is reported by King and Prosser (28). The cylinder was displaced and released, and the resulting logarithmic decrement recorded over a range of velocities (Fig. 8). From the initial still water value, δ , reduced with increasing velocity, reaching a minimum at the equivalent of $V/nd = 1.2$ and then increasing abruptly for further increases of velocity. This demonstrates that although the hydrodynamic damping was a minimum, the Stability Parameter was large enough to suppress sustained excitation.

2.4 Cross-flow oscillations

The excitation range of cross-flow oscillations in air (29, 30) extends over $4.75 < V/nd < 8$ and maximum amplitudes occur in the range $5.5 < V/nd < 6.5$

In water (4, 31), the excitation range of cross-flow oscillations can be increased to $4.5 < V/nd < 10$ with maximum amplitudes falling within the range of $6.5 < V/nd < 8$.

The differences between the performance in air and water are caused by differences in mass ratio and length/diameter ratio, although test facility details (i.e., damping, boundary effects and turbulence levels) would also influence the results.

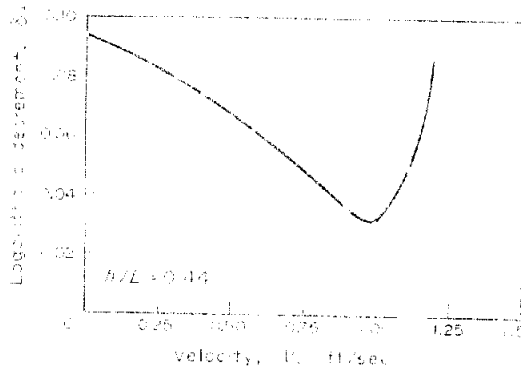


FIG. 8. Stable cylinder: logarithmic decrement in flowing water

The oscillations arise from interactions between the cylinders' flexibility and the mechanisms in which vortices are shed from alternate sides of the cylinder. Figure 9 shows the wake of a cylinder oscillating in the cross-flow direction. The interactions augment circulation in each vortex so that large dimples form in the water surface, as seen in the photograph. The width of the vortex street is a function of the oscillatory amplitudes because a vortex is shed at each crossflow reversal of direction, i.e., each half cycle. Throughout the major part of the excitation range, the frequency of vortex shedding is no longer a function of velocity but is approximately constant and equal to the cylinder's natural frequency (in the case of a cylinder in water, the natural frequency measured in still water). This is the synchronisation described in 2.2. The width (a) and longitudinal spacing (b) of vortices in a fully developed street shed from a stationary cylinder, are theoretically related so as to maintain a constant ratio $a/b = 0.28$ (21) and this has been confirmed by experiment. This apparently also applies to the vortex wakes of oscillating cylinders and the longitudinal spacing adjusts to satisfy the $a/b = 0.28$ condition for each change in oscillatory amplitude (and thus a).

The oscillatory amplitudes are dependent not only upon V/nd but also upon the Stability Parameter K_s as shown in Fig. 10(a), which was compiled from wind tunnel and water channel experimental results and the common curve is of approximately hyperbolic form. The largest amplitudes were recorded for the smaller values of K_s and for a sufficiently large K_s (> 18) the cylinder was virtually stationary. The amplitudes plotted on the graph are the maximum amplitudes mutually experienced by the cylinder and fluid. For cylinders in air flow these are fairly easily defined but for the water channel tests with part-immersed cylinders the amplitudes are functions of mode shape. For the fundamental (sway) mode the largest amplitudes are recorded at the water surface, while for higher normal modes they would be those recorded for the immersed sections. It is not meaningful to quote amplitudes of sections of the cylinders not exposed to the fluid forces because the essentially non-linear and amplitude-dependent flow excitation phenomena are extant only over the common immersed length.

The form of the Stability Parameter also allows for the part-immersed effects by re-defining an equivalent cylinder whose length is equal to the water depth. Consider a vertical cylinder of length L , generalised mass/unit length m_x at x from the bed level and



FIG. 9. Surface flow patterns. Self excited oscillations cross-flow.

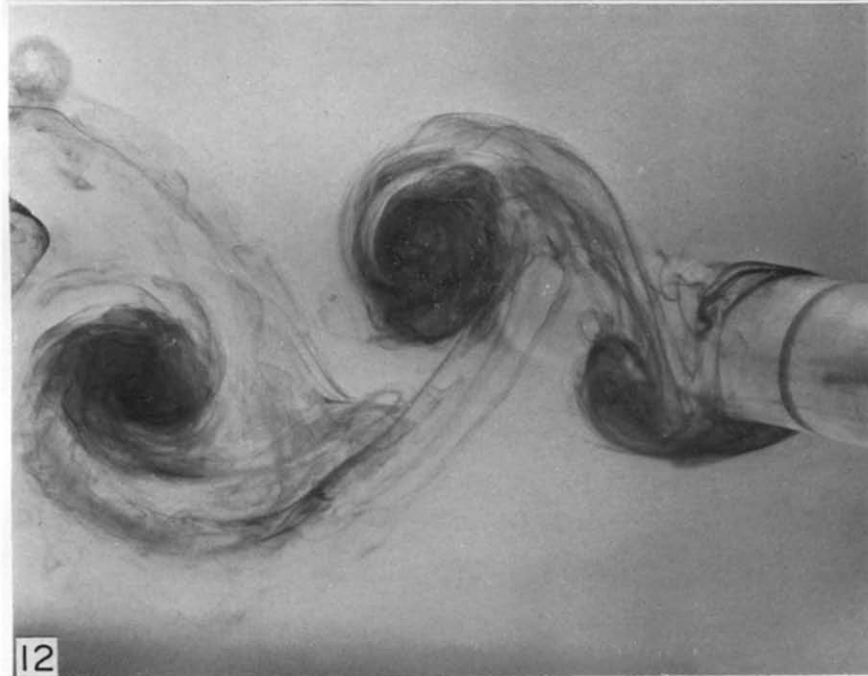
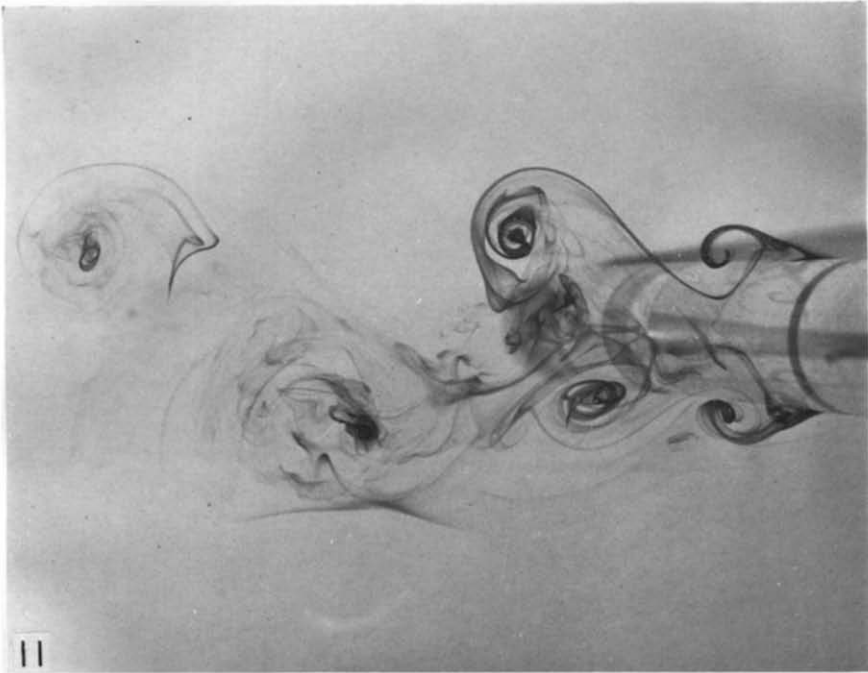


FIG. 11. Symmetric vortex shedding. Self-excited oscillations in-line

FIG. 12. Alternate vortex shedding. Self-excited oscillations cross-flow

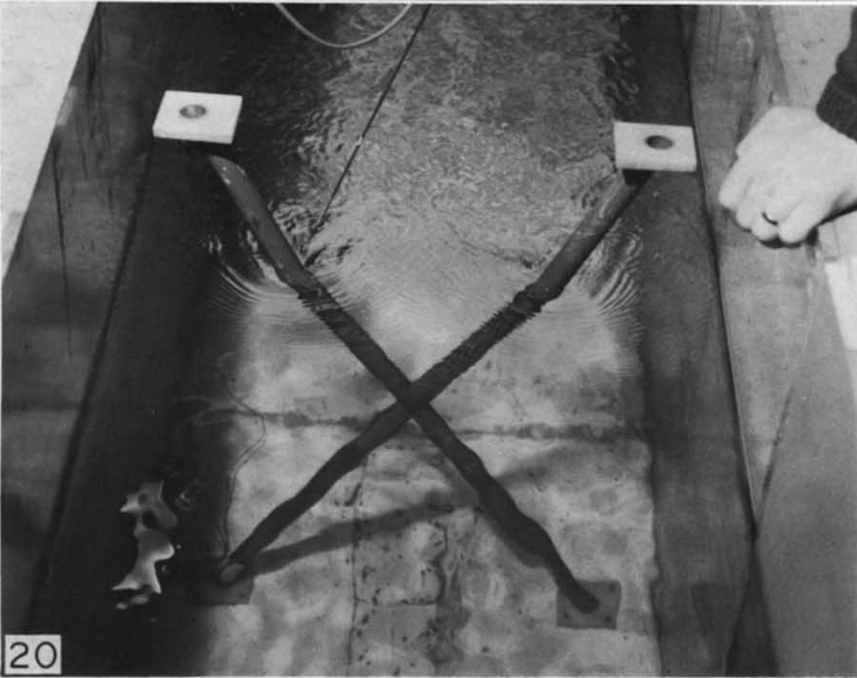


FIG. 18. Self excited oscillations: cylinder with $2d$ long splitter attached.

FIG. 20. The cross-braced frame used in model tests.

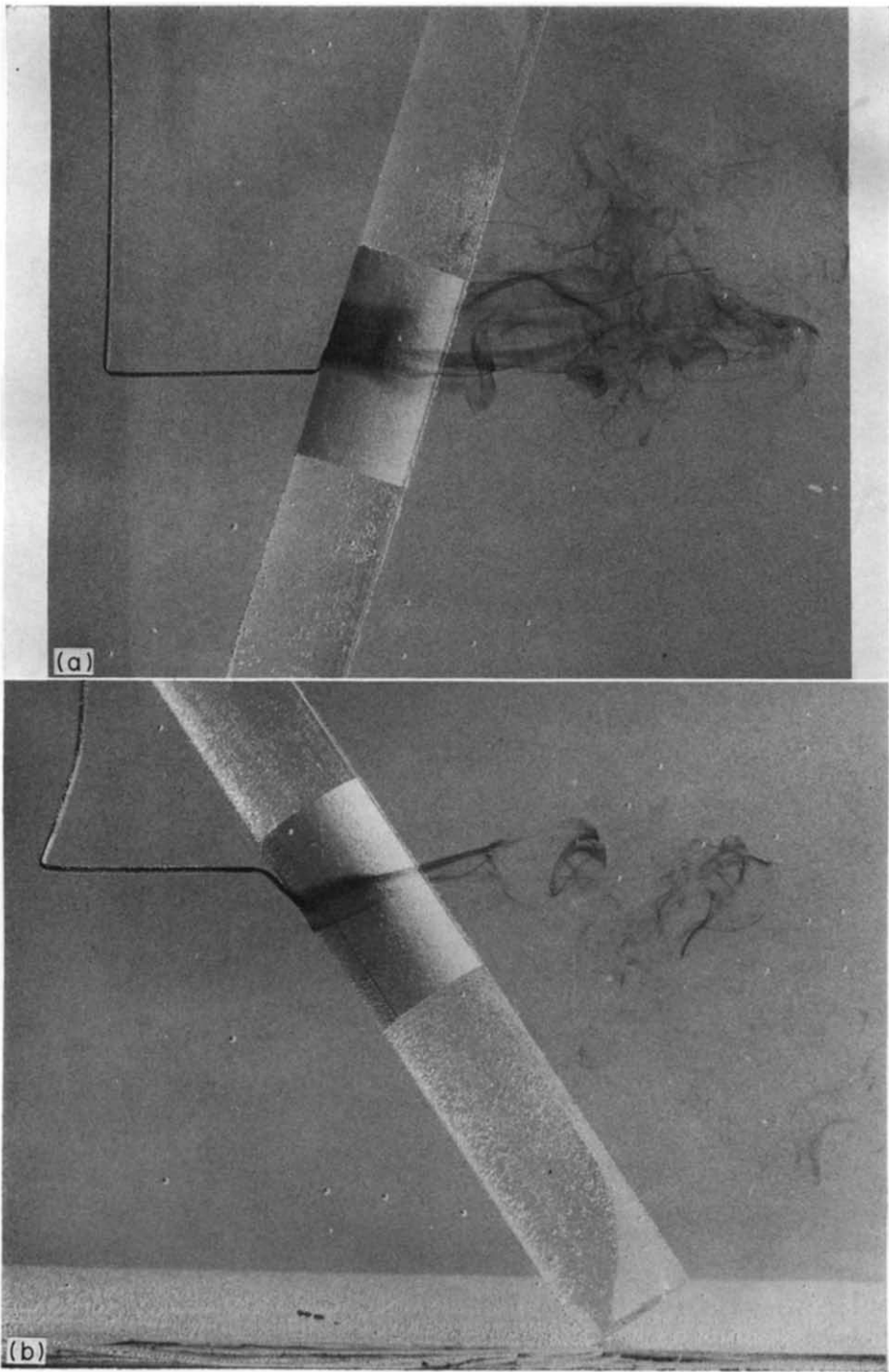


FIG. 19. The effects of inclining a cylinder in a fixed depth of water

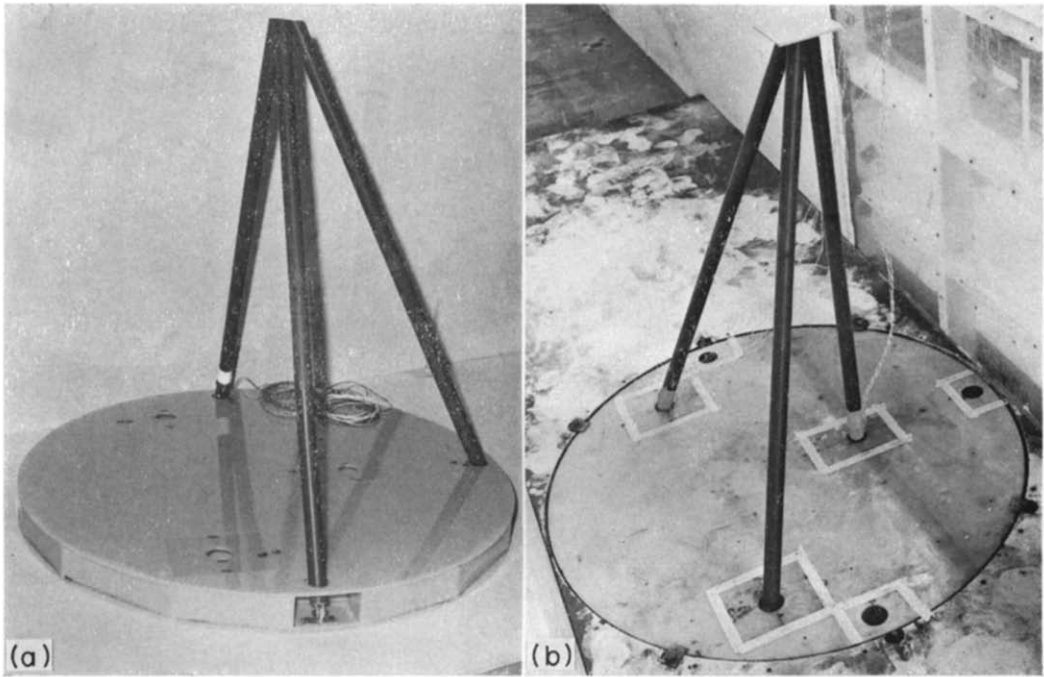


FIG. 21. Hydroelastic model tripods.

having a generalised deflection y_x at x . An equivalent cylinder of length equal to the water depth h but possessing the original quantity of kinetic energy could be defined:

$$\int_0^L \frac{1}{2} m_x (y_x w)^2 dx = \frac{1}{2} m_e \int_0^h (y_x w)^2 dx$$

where $w =$ natural frequency

Thus the equivalent mass/unit length $m_e = \frac{\int_0^L m_x y_x^2 dx}{\int_0^h y_x^2 dx}$.

The term m_x will consist of the cylinder mass/unit length m_s (including internal water m_w if any) and the added mass m_a associated with the outside diameter of the cylinder (see Section 4). This form of m_e can be used in K_s if the in-phase component of fluid force is inertial and invariant with fluid velocity (i.e., if the added mass is constant and ‘frozen’ to the cylinder). Experimental results have confirmed that within limits added mass is not affected by amplitude and frequency (32). Darwin (33) points out that in reality the added mass cannot be regarded rigorously as a collar of fluid surrounding the cylinder as the system is a time-varying one, involving changes in the ‘drift mass’ each half cycle.

From Fig. 10 we can observe that the maximum cross-flow amplitudes are approximately

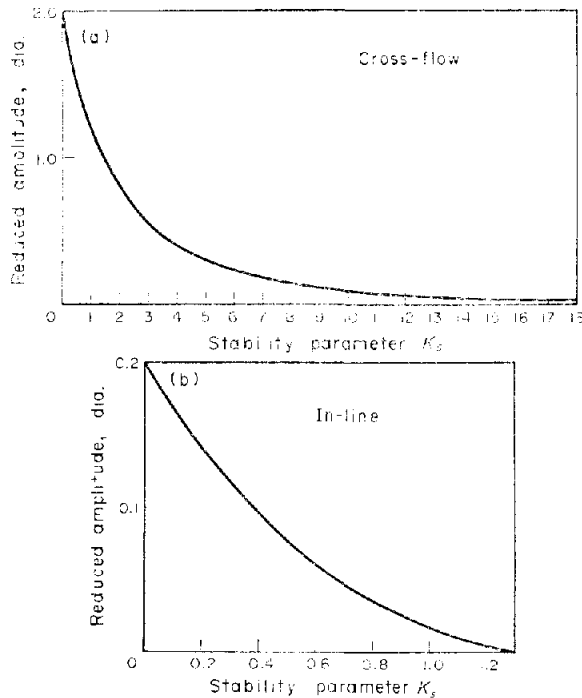


FIG. 10(a). Limiting amplitudes of self-excited oscillations cross-flow.

FIG. 10(b). Limiting amplitudes of self-excited oscillations in-line.

2 diameters, and unlike mechanical oscillations, the amplitudes do not tend to infinity for zero damping. This amplitude dependence is typical of non-linear self-excited oscillations.

2.5 In-line oscillations

Oscillations in the in-line direction are contained within two adjacent but separate instability regions (4). The first instability region covers the range $1.25 < V/nd < 2.5$ and excitation in-line thus is initiated at velocities only one quarter of those necessary for cross-flow excitation (i.e., $V/nd = 1.25$ c.f. $V/nd \approx 5$). Maximum amplitudes coincide with $V/nd \approx 2.1$. The second instability region is $2.7 < V/nd < 3.8$ with maximum amplitudes at $V/nd \approx 3.2$. These values are influenced by the magnitude of K_s , length/diameter ratio and other effects. The amplitudes of oscillation in the two instability regions are approximately equal. Cross-flow oscillations are characterised by exclusively alternate vortex shedding, but these two instability regions of in-line motion are associated with both symmetric and alternate vortex shedding (4). The first instability region is identified by symmetric vortex shedding and the second by alternate vortex shedding (see Figs. 11 and 12). These results are applicable to at least the first three normal modes of cantilever oscillations in-line. A composite graph of successive instability regions of in-line and cross-flow motion may be drawn to a base of flow velocity (Fig. 13).

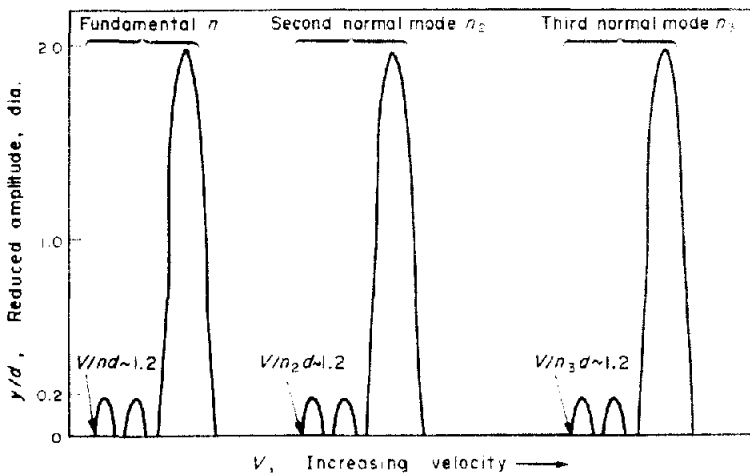


Fig. 13. Composite graph of instability regions in-line and cross-flow.

Figure 10(b) shows the oscillatory amplitude $v K_s$ graph for the first three normal modes of in-line motion. It is similar in shape to Fig. 10(a) and reveals that significant oscillations in-line will be initiated only if $K_s < 1.2$. Maximum amplitudes in-line are approximately 0.2 diameters, or about one-tenth of the corresponding maximum cross-flow amplitudes.

The Stability Parameter K_s plotted in the graphs of Fig. 10 were calculated according to the descriptions in Sections 2.4 and 4.

Although the graph of Fig. 10(b) was compiled from laboratory experiments (26) the results of a full scale test (34) are also included and these fall on the common curve. Hydro-

elastic model testing (10) has previously established the validity of small scale testing of oscillating marine structures.

2.6 Quasi-steady drag forces

(a) *Stationary cylinders (rough and smooth)*. The general trend of drag coefficient C_d v Reynolds numbers for smooth cylinders is given in Fig. 1. Cylinder surface roughness and free stream turbulence can both influence the absolute values on this graph. Fage and Warsap (35) showed that increasing the surface roughness of the cylinder caused the abrupt reduction in C_d in the Critical region to occur at progressively lower Reynolds numbers. They also concluded that free stream turbulence could stabilise the cylinder boundary layer and delay entry into the Critical region (i.e., the opposite effect to increasing roughness). Large surface roughness may cause immediate transition to turbulence in the boundary layer (36) and the spectacular decrease in C_d in the Critical region (Fig. 1) may be reduced to a decrease of 1.2–0.7 at Reynolds numbers as low as $Re = 6 \times 10^4$ compared with $Re = 2 \times 10^6$ for smooth cylinders. Miller (37) has investigated the effects at high Reynolds numbers of roughness on circular members using actual and simulated marine growths. For a heavily fouled space frame structure the local drag coefficients could be as high as 1.0 representing an increase of between 50 and 70% over that for a smooth cylinder. Additionally the loadings could be increased due to increases in the member diameter. Szechenyi (38) has described the use of rough small cylinders to simulate the boundary layers of some larger cylinders at high Reynolds numbers.

From Fig. 1, we can see that $C_d = f(V/S)$, and if this functional relationship remained unaltered for rough cylinders, then roughening the cylinder should cause a variation in the frequency of vortex shedding. However Mujumdar and Douglas (39) have shown that roughening cylinders in the Reynolds number range 4×10^3 – 1.6×10^4 causes negligible variations in shedding frequency even when roughness heights of up to $0.11d$ were used.

(b) *Cylinder oscillating in-line in water*. Laboratory tests in a water channel (26) have shown that at a given velocity (V), the cylinder was deflected elastically from the datum by the dynamic fluid loading equivalent to $\frac{1}{2}\rho V^2 C_d d$ per unit of immersed length. If the cylinder oscillates in-line, the oscillatory motion is superposed on the quasi-steady deflection and the output signals from the strain gauges on the cylinder would register the d.c. shift plus the a.c. component. The 'steady' shift of the base strain gauge recorded in the first instability region in line (26), when plotted against the square of velocity yielded a mean value of $C_d = 1.26$. As a comparison, results of wind tunnel tests at similar Reynolds numbers gave $1.1 < C_d < 1.4$.

Halle and Lawrence (65) have confirmed this superposition of motions for the in-line direction but state that the 'steady' drag forces on a cylinder oscillating in the cross-flow direction increase considerably owing to the increase in frontal area.

2.7 Fluctuating lift and drag coefficients

(a) *Stationary cylinders*. The fluctuating lift and drag coefficients C'_L and C'_d are related to, and deduced from measurements of the fluctuating forces \tilde{F} i.e.:

$$\tilde{F} = \frac{1}{2}\rho V^2 C d \text{ per unit length}$$

where

\tilde{F} is the fluctuating force

C is the fluctuating force coefficient C'_L or C'_d .

The force coefficients are dependent upon Reynolds number, aspect ratio, surface roughness, turbulence and boundary effects. Wide variation of forces can be measured on apparently identical cylinders in different test facilities. Additionally, if the forces are measured on very short instrumented lengths of cylinder comparable with, or shorter than, the vortex correlation length, the total distributed forces can be overestimated (see Section 2.1).

Table 2 lists the fluctuating force coefficients and the corresponding Reynolds numbers. There is considerable scatter between the values quoted and the problem for any designer would be to decide which C'_L or C'_d to select for a particular application. Probably the safest approach is to assume $C'_L \approx 1.2$ and $C'_d \approx 0.2$ for all Reynolds numbers.

TABLE 2. COLLECTED EXPERIMENTAL DATA FROM VARIOUS SOURCES FLUCTUATING FORCE COEFFICIENTS AND REYNOLDS NUMBERS

Source	R.M.S. fluctuating lift Coefficient C'_L	Ratio C'_L/C'_d	Reynolds number range
Jones (64)	0.08		0.4×10^6 – 1.9×10^7
McGregor (22)	0.60	10	4.3×10^4 – 1.3×10^6
Surry (23)	0.60	2.5–10	4.4×10^4
Bishop and Hassan (19)	0.60	10	3.6×10^3 – 1.1×10^4
Ruedy (55)	0.93		Approx. 10^5
Woodruff and Kozak (56)	0.65		0.2×10^6
Vickery and Watkins (7)	0.78		10^4
King (26)	0.78	5.7–10	4×10^4
Fung (57)	0.20–0.30	10	0.2×10^6
Glenny (58)		3	0.2×10^6
Keefe (14)	0.43	10	4×10^4 – 10^6
Humphreys (13)	0.30–1.35		3×10^3 – 5×10^4
Phillips (61)	0.75		200
Schwabe (62)	0.45		Approx. 700
Protos <i>et al.</i> (63)	0.30		4.5×10^4

(b) *Oscillating cylinders.* The coefficients are deduced from experimental force measurements on the oscillating cylinders and compared with results from linear or non-linear mathematical models of the fluid/cylinder system. The results derived in this way are critically dependent upon the type and complexity of the mathematical analogues.

Figures 14(a), (b) and (c), are graphs of equivalent fluctuating lift and drag coefficients against amplitudes of oscillation for the in-line and cross-flow directions (7, 54, 26). Figure 14(a) clearly shows that at low amplitudes the lift coefficient increases with increasing amplitude. As the amplitude rises above 0.5 diameters (considered as the point at which the oscillating cylinder is fully correlated) the lift coefficient begins to decrease (see also (19)) and approaches zero as the amplitude exceeds about one diameter. This gives a limiting amplitude of vortex-excited oscillation that Blevins and Burton (54) considered independent of structural damping although King (26) did not wholly support this view. Nevertheless, the existence of the limit implies that the vortex strength may be self-limiting, as suggested by at least one analytical model (54).

The graphs of drag coefficients for cylinders oscillating in the two instability regions in-line are self-explanatory and show C'_d increasing linearly with amplitude. Unlike the cross-flow results, the amplitudes do not tend to a finite limiting value although in practice

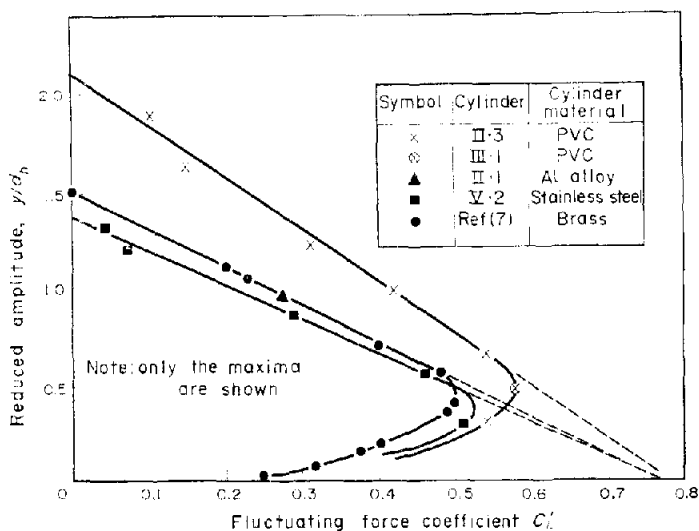


FIG. 14(a). Fluctuating lift coefficients versus amplitudes of oscillation cross flow.

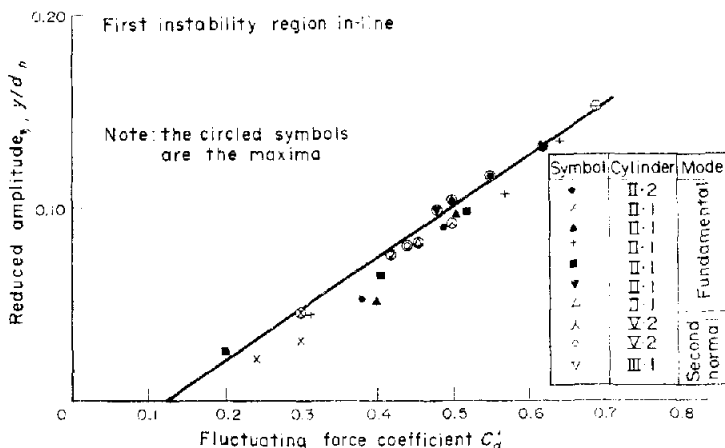


FIG. 14(b). Fluctuating drag coefficients versus amplitudes of oscillation in-line. First instability region.

the maximum amplitudes recorded are of the order 0.2 diameters (26). As with all calculated results, they are of future use only if the original methods of analysis are employed; frequently these methods are extremely complex, although the dynamic behaviour can be predicted accurately (40), (54). Figure 10 offers the most convenient method of assessing the oscillatory stresses; the Stability Parameter, K_s must first be calculated and the corresponding maximum oscillatory amplitude is then read from the appropriate graph. Stress levels equivalent to this amplitude are then calculated using standard theory (see example in Section 4).

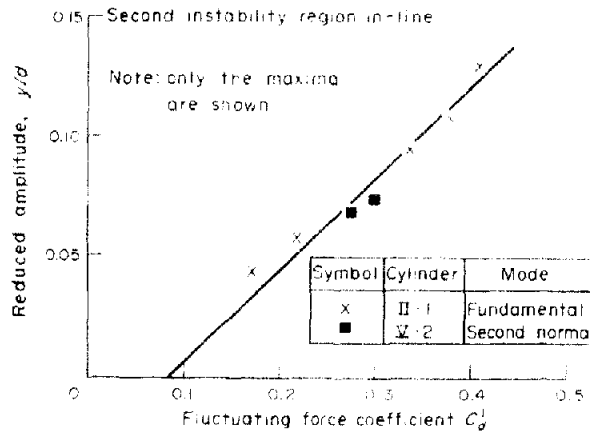


FIG. 14(c). Fluctuating drag co-efficients versus amplitudes of oscillation in-line. Second instability region.

2.8 Blockage effects of cylinders

Probably the most extensive tests on blockage effects of cylinders are those of Ramamurthy and Ng (41) who investigated blockage ratios in the range $0.07 < d/B < 0.7$ for Reynolds numbers up to 2.3×10^6 . Figures 15 and 16, show the way in which blockage ratios can influence the steady drag coefficients and also the Strouhal number of vortex shedding (41). The values of C_d show sensitivity to Reynolds number only at the higher d/B (Fig. 15(a)). When the mean gap velocity is used as the characteristic velocity in defining the drag coefficient, the results collapse on to a single line (Fig. 15(b)) which maintains a reasonably constant value until the flow around the cylinder attains the critical Reynolds number for a given blockage. The curve then drops abruptly as predicted from tests with isolated cylinders. The results also imply that the critical Reynolds number is reached much earlier for the higher blockage ratios.

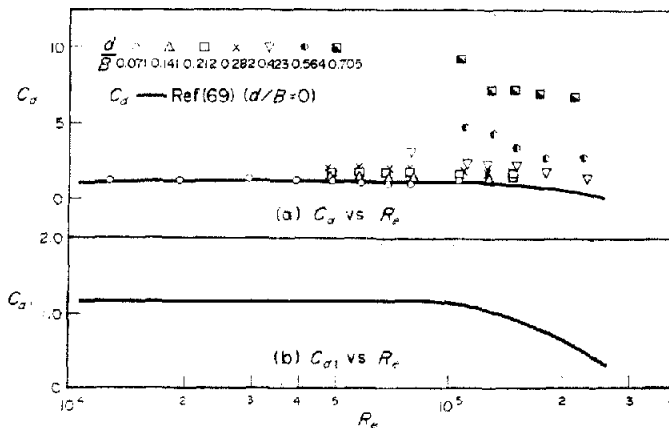


FIG. 15. Drag coefficients versus blockage ratios, calculated using free stream velocity (15(a)) and gap velocity (15(b)).

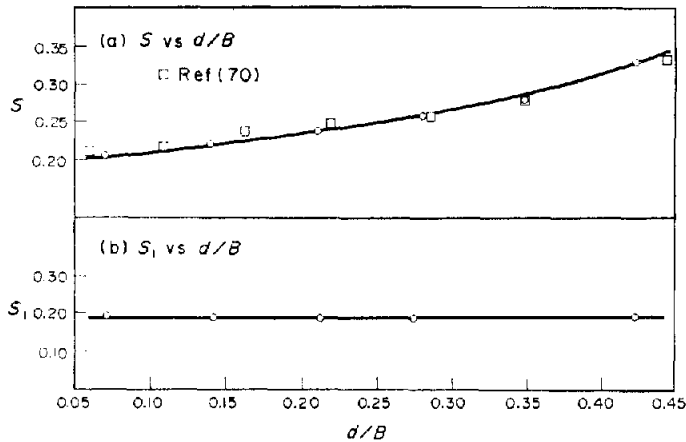


FIG. 16. Strouhal number versus blockage ratios, calculated using free-stream velocity (16(a)) and gap velocity (16(b)).

Figure 16(a) shows Strouhal number plotted against blockage ratios using the free-stream velocities, the cylinder diameter and the experimentally recorded values of vortex shedding frequencies to define S . There is a systematic increase in the Strouhal number with increased flow constriction although no significant Reynolds number effects were apparent. In Fig. 16(b), the Strouhal number is replotted in terms of the mean gap velocity against blockage ratio. This shows that for the subcritical region, the Strouhal number is constant for all blockage ratios up to $d/B = 0.42$. Ramamurthy and Ng (41) make the comment that caution should be used in physically modelling the flows. Dynamic similarity cannot be achieved by the use of a fixed blockage ratio with an adjusted mean gap velocity because the accelerations along the forebodies are themselves controlled by the blockage.

3. WAKE INTERFERENCE TESTS

As a further means of illustrating the mechanisms involved in sustaining the oscillation discussed, a splitter plate and a second identical cylinder were placed in sequence in the wake of a flexible cylinder.

The splitter used was a brass sheet 1.5mm thick extending for six diameters in the direction of flow. It was set in the wake of a 2.5 mm dia., 1000 mm long P.V.C. cylinder, and the gap (Z) between it and the cylinder could be varied $d/16 < Z < 6d$ (42).

For the cylinder-cylinder tests, the cylinders were clamped to separate bases and located relative to each other along a common centre-line with a variable gap G such that $0.25 < G/d < 6$ (47).

3.1 Cylinder-splitter tests

The results for the in-line direction are assembled in Fig. 17. The isolated cylinder results (i.e., no splitter) show the characteristic two instability regions; the first is identified by symmetric vortex shedding and the second by alternate vortex shedding (see Section 2.5). The cylinder-splitter results were recorded when the splitter was placed in the wake with a gap $Z = d/8$. Over the range $1.4 < V/nd < 2.3$ the two sets of results of cylinder oscillations are reasonably similar, both quantitatively and qualitatively. However, for values of

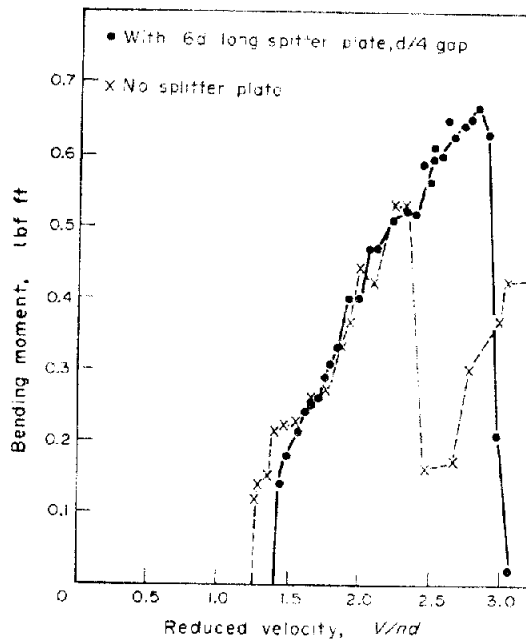


FIG. 17. Wake interference tests. Cylinder-splitter results superposed on isolated cylinder results.

Reduced Velocity greater than 2.3, fundamental differences are evident. The splitter effectively extends the first instability region, increases the cylinder's amplitudes of oscillations and suppresses the establishment of a second instability region. Not unreasonably the splitter assists the formation of symmetric vortices and suppresses the formation of alternate vortices (see also (66)). Figure 18 shows the cylinder with a $2d$ long splitter attached, undergoing self-excited oscillations in the in-line direction. The vortices are shed symmetrically and maintain an approximately symmetric disposition along the splitter before forming an alternate wake downstream.

The cross-flow mode behaviour of the cylinder-splitter arrangement is extremely complex.

For a gap in the range $d/16 < Z < d/8$ the cylinder remained stationary throughout the excitation range of the isolated cylinder $5 < V/nd < 7$. As the velocity was increased further, violent self-excited large amplitude oscillations were initiated abruptly at $V/nd \approx 9$. The amplitudes of these oscillations were considerably larger than those of the isolated cylinder. When the cylinder was deflected and released, in the range $6 < V/nd < 8.5$, the logarithmic decrement of this transient motion decreased rapidly and this is similar to the effect recorded in the isolated cylinder tests of Fig. 8.

For increasing spacings in the range $d/8 < Z < 2d$, the threshold of the violent large amplitude oscillations coincided with progressively lower values of V/nd ; the violence of the onset of instability also decreased and the isolated cylinder situation was approached for $Z \approx 2d$.

Sallet (66) describes the stabilising effect of a splitter plate fixed to a cylinder and explains the way in which the splitter operates in terms of the stability of the laminar

symmetric vortices, called Föppl vortices. He suggests that the length (projection) of the splitter plate is a function of the L/d of the cylinder and that for short cylinders ($L/d \approx 5$) splitters $3d$ long should be sufficient to suppress cylinder cross-flow motion.

Sallet's tests were conducted with short cylinders and end effects would be unavoidable; the extrapolation of these results to longer cylinders is not necessarily valid.

Roshko (67) has studied the vortex shedding frequencies from a rigid cylinder with a splitter either attached or placed at varying distances downstream. A $1.14d$ long splitter placed with a gap of $2.66d$ caused a reduction in Strouhal number from $S = 0.21$ to $S = 0.12$ at Reynolds numbers up to 1.53×10^4 . However, for gaps greater than $2.66d$ the vortex shedding frequency increased abruptly to just below the isolated cylinder value. This indicates that for the short splitter plate the isolated cylinder situation was approached for $Z \approx 2.7d$, compared with $Z \approx 2d$ for the longer ($6d$) splitter plate (42).

3.2 Cylinder-cylinder tests

(a) *Rigid cylinders.* Experimenters (43, 44, 45) have shown that considerable wake interaction is generated between cylinders closely spaced in-line, and for $0 < G/d < 1$, negative drag forces can be detected at the downstream cylinder. For $1 < G/d < 3$ it is reported that fluctuating lift and drag forces of the same order as the steady drag forces can be created (43). The isolated cylinder situation is approached for $7 < G/d < 15$ (44, 46).

(b) *Oscillating cylinders.* Due to the complexity of the overall behaviour recorded in the cylinder-cylinder tests particularly when they were coupled together elastically, the conclusions reached by King and Johns (47) will be reproduced in full.

"When two identical cylinders are partly or wholly immersed in a flowing fluid and spaced at between 0.25 and 6 diameters in the flow direction, complex mutual interactions can arise between the flow, the vortex wakes and the deflections of the cylinders. The oscillatory response of the cylinders primarily is a function of G/d , V_r/nd and the stability parameter K_s (it is also dependent upon Reynolds number; Re must exceed 1200–1500 or in-line oscillations will not be induced (10); these are excited by symmetric vortices probably created from secondary vortices which do not form below a minimum $Re = 1250$ (4); for oscillations in the cross-flow direction, the Reynolds number must exceed 100). If the cylinders are structurally uncoupled the motion of each depends upon their spacing and the nature of the wake interactions; in particular, the amplitude of the downstream cylinder is strongly influenced by the way in which the vortices are shed from the upstream cylinder. If the gap between the uncoupled cylinders is less than 1.75 diameters, symmetric vortices are shed from both cylinders in the range $1.25 < V_r/nd < 2.5$ and both cylinders will oscillate in the in-line direction provided the stability parameter of each is less than $K_s = 1.2$. If $G/d > 1.75$ and $1.25 < V_r < 2.5$, the upstream cylinder may oscillate with sustained large amplitudes in the in-line direction whilst the downstream cylinder remains stationary, and this observation applies to the second normal mode in addition to the fundamental (sway) mode of oscillations in-line if the gap (G) between the cylinders exceeds 2 diameters. Tentatively this is explained in the text by a consideration of symmetric and alternate vortex shedding, both of which can be generated during sustained self-excited oscillations in the in-line direction. This reasoning is supported by photographs of the vortex shedding processes. When $2.7 < V_r < 3.8$, the alternate vortex wake from the upstream cylinder generally reinforces that from the downstream cylinder and for all spacings $0.5 < G/d < 6$ the rear cylinder oscillates with an amplitude greater than that of

the leading cylinder. If the upstream cylinder is held stationary, the oscillatory in-line amplitude of the downstream cylinder is greatly reduced. However, one cylinder is capable of driving both flexible cylinders (if they are structurally coupled) provided the sum of their stability parameters is less than the critical value $K_{sc} \approx 1.2$. Although there is no previous research with which to compare these results directly, the ranges of spacings for mutual interaction quoted above are of an order similar to those recorded on stationary cylinders.

Motion in the cross-flow direction is less dependent upon the cylinder spacing for $0.25 < G/d < 6$ and it appears that the alternate vortex shedding from the oscillating upstream cylinder generally reinforces that from the downstream cylinder. Coupling the cylinders together normally leads to a greater level of excitation in the cross-flow direction.

The discontinuity in the drag vs spacing curve (in the region $2.5 < G/d < 3$) noted by some authors, was not observed in the present tests, in either the in-line or cross-flow directions.

An analysis of the overall results, based on Owen's discussion (49) of the flow-induced instability of cooling tower arrays failed to establish any well-ordered relationships in the data. However, in his paper, Owen considered the amplitudes of the cooling towers to be small compared with their diameters, and this assumption alone may exclude the large amplitude results recorded here from such analysis.

Although the range in which interactions were recorded in the present tests (47) were within the spacing range for buffeting-type fluctuations, the explanation based on vortex wake degeneration is considered more plausible for sustained oscillations."

3.3 *Inclined cylinders, plane and 3-d frames*

Inclining a cylinder at an angle ϕ from the vertical relative to the flow direction has the dual effect of increasing the cylinder's wetted length (for a fixed depth of water) and decreasing the local flow velocity component (Fig. 19). An increase of wetted length results in a lowering of natural frequency and an increase of Reduced Velocity, thus making the cylinder more liable to excitation. However, this is offset to some extent by the reduction in velocity component. In calculating the Reduced Velocity, the velocity component $V \cos \phi$ should be used; the true wetted length is the upper limit for the integration of the mode shape for defining K_s . The frequency n should be calculated with an allowance for the increased wetted length.

The criteria to be satisfied to achieve stability for angles $-45^\circ < \phi < +45^\circ$ are:

$$\begin{aligned} V \cos \phi / nd < 1.2, K_s > 1.2 \text{ in-line;} \\ V \cos \phi / nd < 4.5, K_s > 17 \text{ cross-flow (50).} \end{aligned}$$

Plane frames and a three-dimensional structure both fabricated from inclined members have been tested (see Figs. 20 and 21 and Refs. 50, 51, 17); in general the amplitudes of oscillation could be predicted from the isolated inclined cylinder data. Figure 22 shows the response of these frames superposed on the isolated cylinder graphs.

4. SUPPRESSION OF VIBRATIONS IN STEADY CURRENTS (TAKEN FROM REF. 52)

4.1 *Design approach*

The two criteria governing the onset of vibrations are the Reduced Velocity V_r and the Stability Parameter K_s . Both criteria must be satisfied simultaneously for vibrations to be excited. Figure 13 defines the relationship between vibrational amplitudes and V_r ; vibrations

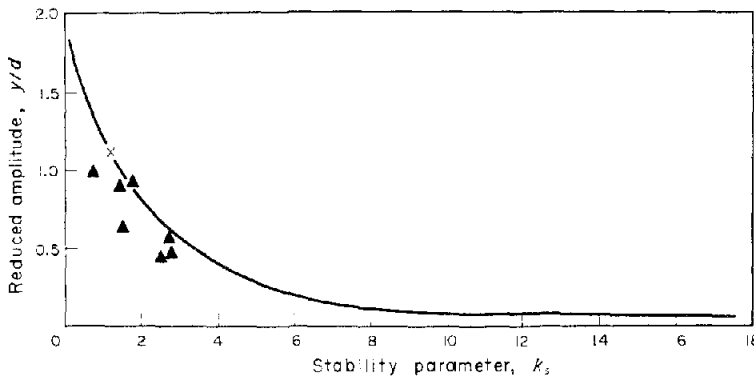


FIG. 22. Oscillatory amplitudes of the cross-braced frame superposed on graphs from isolated vertical cylinders.

can be excited in the in-line direction for $V_r > 1.2$ and in the cross-flow direction for $V_r > 3.5$. Figure 10 shows the variation of vibrational amplitude with K_s ; the limiting amplitudes as K_s tends to zero are about 0.2 diameters in-line and 2 diameters cross-flow. Alternatively, motion can be virtually suppressed if K_s exceeds about 1.2 in-line and about 18 cross-flow.

In calculating the natural frequency n of a cylinder in water, allowances must be made for the external added mass of water and the mass of water inside the cylinder. For a thin-walled cylinder, assume that both are equal to the mass of water displaced by the outside diameter.

First, assume that the cylinder is completely immersed i.e., $m_e = m_s + m_a + m_w$ and calculate n from standard beam theory, for the main modes of practical interest. For a completed structure with a cap mass, the sway mode can be calculated as for a cantilever, making an allowance for the cap mass supported by each pile. Each frequency in sequence should be checked in the appropriate V_r criterion to determine whether or not vibrations are likely. In calculating the Stability Parameter K_s for each mode, assume initially that $\delta \approx 0.1$ for steel members. As a more accurate check for part-immersed members use Figure 23 to calculate m_e for each mode.

For the fundamental sway mode:

$$m_e = 4.2 \frac{M_t}{L} \gamma + m_s \gamma + m_a + m_w$$

and for the clamped-pinned and clamped-clamped modes:

$$m_e = \gamma m_s + m_a + m_w$$

γ is the integral ratio appropriate to each h/L shown in Fig. 23. If the calculated K_s is less than 1.2 and $V_r > 1.2$ or > 3.5 , use the graphs of Fig. 10 to determine the equivalent vibrational amplitudes likely to be excited. These graphs can be applied to plane frames and 3-dimensional structures, although wake interactions and proximity effects can modify

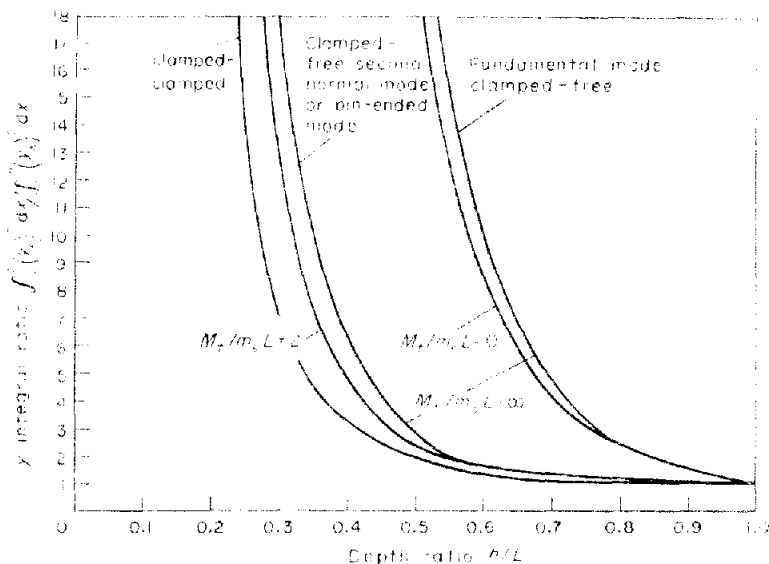


FIG. 23. The integral ratio as a function of water depth h/L , used to calculate K_s .

both the amplitudes and the criteria if the members are closely spaced. If the amplitudes exceed acceptable levels, some redesigning may be necessary.

The application of the design criteria. To illustrate the use of the stability criteria, Table 3 contains details of full scale and model structures.

The model structure was formed from a pair of tripods, used in recent hydroelastic model tests at BHRA Fluid Engineering on a proposed design of ship jetty. The jetty design incorporated groups of piles arranged in tripods to form the main structure: each tripod consisted of three raked piles. The model piles were 38 mm dia., with the elasticity and mass distribution of the prototype represented by suitable choice of model materials.

In Table 3 the two stability criteria were satisfied in only three locations and of these only structure 1 oscillated appreciably. The K_s of structure 2 implies that the maximum amplitude possible was only $0.02d$ and this probably accounts for its stable classification.

TABLE 3.

Structure	1	2	3	BHRA Model	5	6	7	8	9
Pile type	Steel tube	Steel tube	Octagonal steel	PVC tube	Octagonal steel	Steel tube	Steel tube	Octagonal steel	Steel tube
V/nd of piles	1.86	0.59	1.06	0.97* 1.33†	0.47	0.83	0.60	0.40	0.77
V/nd sway	4.05	1.64	1.67	1.90	2.8	2.4	0.91	2.5	2.01
K_s of piles	0.27	0.28	0.35	0.31	0.35	0.28	0.27	0.35	0.28
K_s sway	1.61	0.90	1.3	2.97	4.06	2.42	1.93	2.56	1.87

*Vertical piles.

†Raked piles, $V \cos \phi/nd = 1.19$. Note: The full scale results are taken from ref. (68).

The K_s of the bowstring mode of structure 3 was very low and amplitudes of $0.12d$ were theoretically possible for circular section piles. An allowance was made for the influence of the octagonal section of the piles actually used, resulting in $V_r = 1.06$. This is below the threshold and is consistent with the reported stability.

4.2 Use of vortex spoilers

Helical strakes have been used for many years to suppress the cross-flow oscillations of structures (e.g. chimneys) in air. However, piles fitted with strakes create problems in handling or driving and the strake has not been generally adopted for use in water, although it is believed that the 1st World War submarines were fitted with this device to suppress periscope oscillations.

The most advantageous vortex spoilers in water are perforated shrouds and radial fins. The use of perforated shrouds was first suggested in 1956 and tests conducted since then have optimised the shroud geometry (53). This should have a diameter 20% greater than the pile diameter, an open area ratio of about 36% and extend for 20% of the wetted length. In full scale marine tests, a fairly thick growth of crustacea did not reduce the shroud's effectiveness (34).

The radial fin was proposed from tests on full scale vertical piles (34) and the suggested size for this projection was 10% of a diameter extending for 15% of the piles wetted length. On the full scale, these fins were mounted on the pile at an angle of 45° from the front stagnation point. Cable oscillations may be suppressed by the attachment of trailing ribbons (16).

Example in the use of vortex spoilers. Both types of vortex spoiler were evaluated during recent hydroelastic model tests at BHRA on the tripods shown in Fig. 21. Each spoiler in sequence was clamped to one or more of the tripods' raked piles.

The results showed that in some orientations of the tripod to the flow, a shroud on just one or two legs, completely suppressed the response to excitation of the bowstring mode in the in-line direction. In general individual shrouds were less effective when they

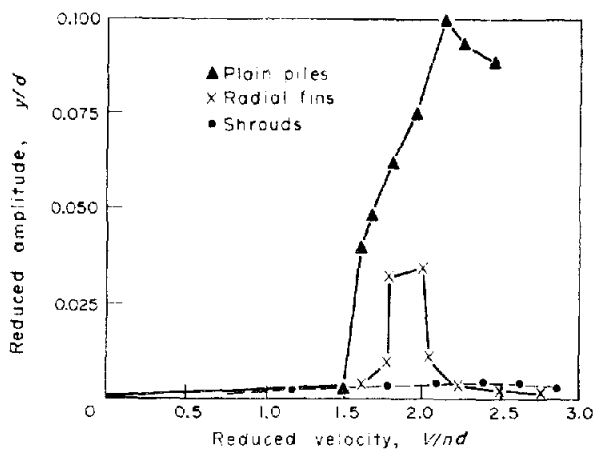


FIG. 24. The effectiveness of clamp-on spoilers used to suppress vortex excitation.

were clamped to a pile that was in the wake of a leading pile, although shrouds on all three piles always prevented the excitation of sustained oscillations.

A single, radial fin clamped on each pile at 45° to the approach flow was not always consistent in suppressing the oscillations. In view of the change of flow directions caused by the ebb and flood tides past the tripods, two fins were mounted on each pile, one at 45° and one at 225° from the front stagnation point. These always suppressed the oscillations. It is considered that the trailing fin was far more efficient than the leading fin and it would seem that the optimum working range of the fin is probably between these two angles. The fin was originally developed from full scale tests with vertical piles and it may be that different angles relative to the flow direction are necessary when the piles are raked. Examples of the effectiveness of the vortex spoiler on the tripod model are shown in Fig. 24.

Acknowledgement—The author acknowledges the permission of the Director and Council of BHRA Fluid Engineering to publish this paper.

REFERENCES

1. KING, R. 1974. Vortex excited structural oscillations of a circular cylinder in steady currents. Paper OTC 1948. *Offshore Technology Conf.* Houston.
2. WALSH, D. E. 1972. Wind excited oscillations of structures. H.M.S.O. Publications S.B.N. 11 480016 2.
3. AUGER, A. 1968. Wind-induced vibration in a space frame structure. *Symp. on Wind Effects on Buildings and Structures*. Loughborough.
4. KING, R., PROSSER, M. J. and JOHNS, D. J. 1973. On Vortex excitation of model piles in water. *J. Sound Vibration* **29** pp. 169–188.
5. RICHARDSON, E. G. The Flow and sound field near a cylinder towed through water. *Appl. Sci. Res.* **A7**, pp. 341–350 (1958).
6. SCRUTON, C. 1963. On the wind-excited oscillations of stacks towers and masts. *Proc. Conf. on Wind Effects on Buildings and Structures*. Teddington.
7. VICKERY, B. J. and WATKINS, R. D. 1962. Flow-induced vibrations of cylindrical structures. *Proc. 1st Australasian Conf.* pp. 213–241.
8. GOUDA, B. H. L. 1975. Some measurements of the phenomena of vortex shedding and induced vibrations of circular cylinders. Technische Universität Berlin Report DLR-FB 75-01.
9. EVERY, M. J. Modelling of marine structures, to be published as a BHRA Report.
10. KING, R. 1974. Hydroelastic model tests of marine piles—a comparison of model and full-scale results. BHRA Report RR 1254.
11. GERLACH, C. R. and DODGE, F. T. 1970. An engineering approach to tube flow-induced vibrations. *Proc. Conf. on Flow-Induced Vibrations in Reactor System Components*. pp. 205–225, Argonne National Laboratory.
12. EL BAROUDI, M. Y. 1960. Measurement of two-point correlations of velocity near a circular cylinder shedding a Karman vortex street. University of Toronto, UTIAS, TN31.
13. HUMPHREYS, J. S. 1960. On a circular cylinder in a steady wind at transition Reynolds numbers. *J. Fluid Mech.* **9**, pp. 603–612.
14. KEEFE, R. T. 1961. An investigation of the fluctuating forces acting on a stationary cylinder in a subsonic stream, and of the associated sound field. UTIAS Report 76.
15. KOOPMAN, G. H. 1967. The vortex wakes of vibrating cylinders at low Reynolds numbers. *J. Fluid Mech.* **28**, pp. 501–512.
16. DIGGS, J. S. A. survey of vortex shedding from circular cylinders with applications toward towed arrays. Technical Report No. 122.
17. KING, R. and EVERY, M. J. 1976. Hydroelastic model tests of two tripod structures for an ore terminal. BHRA Report 1357.
18. BENARD, H. 1907. Formation of the centres of rotation behind a moving object. *C.r. hebdom. Séanc. Acad. Sci., Paris*, **147**, pp. 839–842. (In French).
19. BISHOP, R. E. D. and HASSAN, A. Y. 1963. The lift and drag forces on a circular cylinder in a flowing fluid. *Proc. R. Soc., Lond. A*, **277**, pp. 32–50.
20. UNEMARA, S. 1971. On the vibration of cylinders caused by Karman vortex. *J.S.M.E.* **14**, 75.
21. KARMAN, TH. V. 1912. On the mechanics of resistance experienced by a body moving through a fluid. *Göttinger Nach.* **13**, pp. 547–562.

22. MCGREGOR, D. M. June 1957. An experimental investigation of the oscillating pressures on a circular cylinder in a fluid stream. UTIAS Tech. Note 14.
23. SURRY, D. 1969. The effect of high intensity turbulence on the aerodynamics of a rigid circular cylinder at subcritical Reynolds numbers. UTIAS Report 142.
24. KING, R. 1972. The hydrodynamic damping of natural vibrations of a cantilevered cylinder. BHRA Report 1122.
25. STUART, J. T. and WOODGATE, L. 1955. Experimental study of aerodynamic damping on a vibrating circular cylinder. *Phil. Mag.* **26**, pp. 40–46.
26. KING, R. 1974. Vortex excited structural oscillations of a circular cylinder in flowing water. Ph.D. Thesis, Loughborough University.
27. ZDRAVKOVICH, M. M. 1972. Flow induced vibrations of two cylinders in tandem and their suppression. Paper E7, *I.U.T.A.M./I.A.H.R. Symp. on Flow Induced Structural Vibrations*. Karlsruhe.
28. KING, R. and PROSSER, M. J. 1972. Criteria for flow-induced oscillations of cantilevered cylinders in water. *I.U.T.A.M./I.A.H.R. Symp. on Flow Induced Structural Vibrations*, Karlsruhe.
29. BLEVINS, R. 1972. Vortex induced vibration of circular cylindrical structures. *A.S.M.E. Paper* 72-WA/FE-39.
30. GLASS, R. J. and SAYRE, C. L. JR. 1967. Amplitude and frequency response, and laws of similitude for vortex-excited vibrations of spring supported cylinders in subcritical flow. *1st Canadian Cong. on Applied Mechanics*.
31. GLASS, R. J. 1970. A study of the hydroelastic vibrations of spring supported cylinders in a steady fluid stream due to vortex shedding. Ohio Univ. Ada, Project No. N.00014-69-C-0148.
32. KING, R. 1971. The added mass of cylinders. BHRA Report TN1100.
33. DARWIN, C. Note on hydromechanics. *Proc. Cambridge Phil Soc.* **49**, pp. 342–354.
34. WOOTTON, L. R. 1972. Oscillations of piles in marine structures. C.I.R.I.A. Report 40.
35. FAGE, A. and WARSAP, J. H. 1923. The effect of turbulence and surface roughness on the drag of a circular cylinder. *Aero. Res. Comm. Reports and Mem.* 1283.
36. ACHENBACH, E. 1971. Influence of surface roughness on the crossflow around a circular cylinder. *J. Fluid Mech.* **46**, pp. 321–335.
37. MILLER, B. L. 1975. The drag of roughened cylinders at high Reynolds numbers. National Physical Laboratory Report Mar. Sci. R 132.
38. SZECHENYI, E. 1975. Supercritical Reynolds number simulation for two-dimensional flow over circular cylinders. *J.F.M.* **70**, pp. 529–543.
39. MUJUMDAR, A. S. and DOUGLAS, W. J. M. 1973. Vortex shedding from slender cylinders of various cross sections. *Trans. ASME J. Fluids Engng.* pp. 474–475
40. SKOP, A. and GRIFFIN, O. M. 1973. An heuristic model for determining flow-induced vibrations of offshore structures. Paper OTC 1843 *Offshore Tech. Conf.* Houston.
41. RAMAMURTHY, A. S. and NG, C. P. 1973. Effect of blockage on steady force coefficients. *Proc. ASCE. EM4*, pp. 755–772.
42. KING, R. Unpublished work.
43. LAIRD, A. D. K. 1960. Water eddy forces on oscillating cylinders. *ASCE J. Hyd. Div.* **86**, pp. 43–54
44. NAGAI, S. and KURATA, K. 1971. Interference between cylinders in an open channel flow. *Trans. Jap. Soc. CW. Engng.* **3**, pp. 200–201.
45. BIERMANN, D. W. A. 1933. The interaction between struts and cylinders in various combinations. NACA Report 468.
46. LAIRD, A. D. K. and WARREN, R. P. 1963. Groups of vertical cylinder oscillating in water. *J. Engng Mech. Div. Proc.* **88**, pp. 25–35.
47. KING, R. and JOHNS, D. J. 1976. Wake interaction experiments with two flexible circular cylinders in flowing water. *J. Sound Vibration* **45**, pp. 259–283.
48. KING, R. and BRUCE, B. A. 1975. On the existence of two forms of vortex street shed from immersed solids. BHRA Translation T 1299.
49. OWEN, P. R. 1967. Some aerodynamic problems of grouped cooling towers. *Inst. Civil Engrs Paper* 8 Session 3, National Draught Cooling Towers Ferrybridge.
50. KING, R. 1976. Vortex excited oscillations of yawed circular cylinders. *ASME, Fluids Engng Div.* paper 76-WA/FE 16.
51. KING, R. 1976. Hydroelastic oscillations of a plane cruciform frame. BHRA Report RR1361.
52. KING, R., PROSSER, M. J. and VERLEY, R. L. P. 1976. The suppression of structural vibrations induced by currents & waves. *Proc. B.O.S.S. Conf.* Trondheim, Norway. Paper 2.11, pp. 263–284.
53. PRICE, P. 1956. The suppression of fluid-induced vibration of circular cylinders. *Proc. ASCE, Paper* 1030, **82**, EM3.
54. BLEVINS, R. D. and BURTON, T. E. 1975. Fluid forces induced by vortex shedding. *ASME Paper* 75-FE-10.
55. RUEDY, R. 1935. Vibrations of power lines in a steady wind. *Can. J. Res.* **13**, A.